Design of mechanical components for vibration reduction in an atomic force microscope

Chulsoo Kim, Jongkyu Jung, Woosub Youm, and Kyihwan Park[a)]
Department of Mechatronics, Gwangju Institute of Science and Technology, 261 Cheomdan-gwagiro (Oryong-dong), Buk-gu, Gwangju 500-712, South Korea

(Received 13 July 2010; accepted 5 December 2010; published online 2 March 2011)

Vibration is a key factor to be considered when designing the mechanical components of a high precision and high speed atomic force microscope (AFM). It is required to design the mechanical components so that they have resonant frequencies higher than the external and internal vibration frequencies. In this work, the mechanical vibration in a conventional AFM system is analyzed by considering its mechanical components, and a vibration reduction is then achieved by reconfiguring the mechanical components. To analyze the mechanical vibration, a schematic of the lumped model of the AFM system is derived and the vibrational influences of the AFM components are experimentally examined. Based on this vibration analysis, a reconfigured AFM system is proposed and its effects are compared to a conventional system through a series of simulations and experiments. © *2011 American Institute of Physics*. [doi:10.1063/1.3531948]

I. INTRODUCTION

An atomic force microscope (AFM) is a device capable of investigating several physical characteristics of a material with subnanometer resolution using the interaction force between the cantilever tip and a sample surface.[1–3] There are many factors to be considered for designing the mechanical components for a high speed and high precision AFM, though vibration is one of most influential factors since performance of the AFM can be degraded by vibration in the mechanical components caused by various external and internal vibration sources. As high speeds are required in the AFM, the vibrational influence on precision also significantly increases.

External vibration includes vibrations from operator footsteps, building vibration, seismic waves, and acoustic noise, whose frequencies are usually in a low frequency range, whereas internal vibration includes controller signals whose frequency ranges up to several hundred hertz. Therefore, mechanical components must be designed to have resonant frequencies higher than both the external and internal vibration frequencies. To this end, Thompson *et al.*,[4] Chen *et al.*,[5] and Kindt *et al.*[6] have reported that the mechanical loop between the tip and sample should be designed to have a high first resonant frequency to ensure that it is not affected by the external and internal vibration frequencies. In further attempts to increase the first resonant frequency of the scanning actuator, Schitter *et al.*[7] and Fantner *et al.*[8] proposed a method for enhancing the stiffness of the scanning actuator by adding an array of vertical blade springs to a flexure mechanism, and Fleming *et al.*[9] proposed to replace the vertical positioning function of the piezoelectric tube (PZT) scanner with a high speed PZT stack actuator.

There are two different mechanical configurations that have been used in the AFM;[10] *scan-by-probe* type and *scanning-sample* type. The *scan-by-probe* type AFM typically uses a PZT scanner[11] in which XY-axis motion is taken place as well as Z-axis motion. Since a sample is loaded only for measurement to the motorized stage that is usually used for sample approach to the cantilever in the Z direction, a small mass is just added to the motorized stage, which doesn't much affect the dynamics of the motorized stage. If the motorized stage is manufactured with high stiffness, it has a high first natural frequency. Hence, the *scan-by-probe*-type AFM is less sensitive to the external vibration. However, in this mechanical configuration, coupling effects between the XY-axis motion and Z-axis motion make it difficult to control the actuators for accurate positioning in the Z direction and cause bowing artifacts.[12,13] Additionally, it is not easy to install the sensing instrument for the accurate motion in the X and Y directions.[14,15] For the sake of control easiness in the Z direction and accurate sensing motion in the X and Y directions, it is advantageous to take the *scanning-sample*-type AFM (Refs. 16–18) in which the *xy* scanner can be separately made from the *z* scanner. In order to cope with these performances, the *xy* scanner loaded on the motorized stage is usually heavy. The large mass added to the motorized stage can lower its natural frequency. Therefore, the *scanning-sample*-type AFM is more sensitive to the vibration than the *scan-by-probe*-type AFM. The vibration problem considered in this work is restricted to the *scanning-sample*-type AFM.

In order to solve the vibration problem, in this study the mechanical vibration is analyzed by considering all the mechanical components of the AFM including the motorized stage. As a result, vibration reduction is achieved through a reconfiguration of the mechanical components. To analyze the mechanical vibration, a schematic of the lumped model of the AFM system is derived and the vibration influences of the AFM components are experimentally examined. Based on this vibration analysis, a reconfigured AFM system is proposed and subsequently compared to a conventional *scanning-sample*-type AFM.

[a)]Electronic mail: khpark@gist.ac.kr. Telephone: +82-62-715-2391. Fax: +82-62-715-2384.

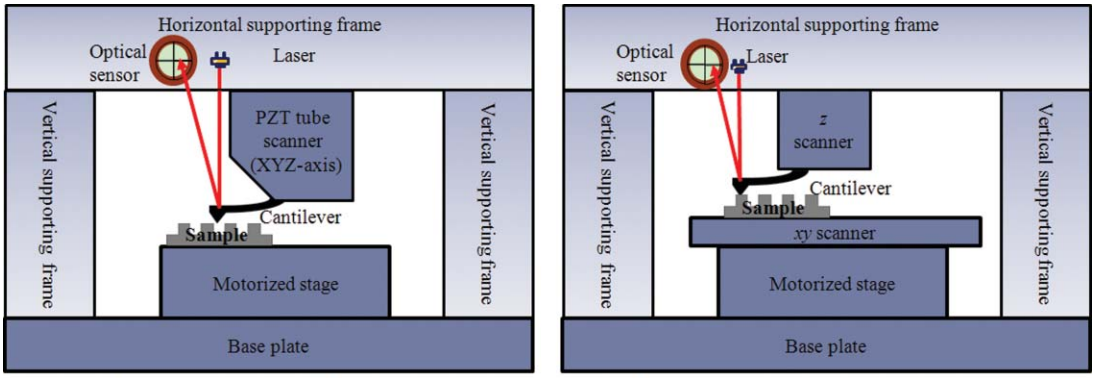

FIG. 1. (Color online) Two different mechanical configurations that have been used in the AFM; (a) *scan-by-probe* type and (b) *scanning-sample* type.

II. MECHANICAL VIBRATION ANALYSIS OF AN AFM

An AFM system is usually composed of a supporting frame, scanning actuator, optical sensor, and motorized stage. The motorized stage makes sample approach to the cantilever tip in the Z direction. The cantilever is deflected by the force between the cantilever tip and the sample surface. This deflection can be conventionally measured using the optical sensor.[19,20] When the scanning actuator moves in the X and Y directions, it is controlled in the Z direction in order to maintain a constant deflection force. The topology of the sample is subsequently obtained from the controlled signal.

There are two different mechanical configurations that have been used in the AFM as shown in Figs. 1(a) and 1(b); *scan-by-probe* type [Fig. 1(a)] and *scanning-sample* type [Fig. 1(b)]. A PZT scanner is typically used in the *scan-by-probe*-type AFM as shown in Fig. 1(a) in which XY-axis motion is taken place as well as Z-axis motion. Since a sample is only for measurement loaded to the motorized stage, a small mass is just added to it, which does not much affect the dynamics of the motorized stage. If it is manufactured with high stiffness, it has a high natural frequency. Hence, the *scan-by-probe*-type AFM is less sensitive to the external vibration. However, in this mechanical configuration, coupling effects between the XY-axis motion and Z-axis motion make it difficult to control the actuators for accurate positioning in the Z direction. Additionally, it is not easy to install the sensing instrument for the accurate motion in the X and Y directions. For the sake of control easiness in the Z direction and accurate sensing motion in the X and Y directions, it is advantageous to take the *scanning-sample*-type AFM as shown in Fig. 1(b) in which the *xy* scanner can be separately made from the *z* scanner. In order to cope with these performances, the *xy* scanner loaded on the motorized stage is usually heavy. The large mass added to the motorized stage can lower its natural frequency. Therefore, the *scanning-sample*-type AFM is more sensitive to the vibration than the *scan-by-probe*-type AFM. The vibration problem in this work is restricted to the *scanning-sample*-type AFM.

Figures 2(a) and 2(b) show the structure and schematic of the lumped model of the motorized stage, respectively, comprised of a linear motion block, lead screw, motorized stage, and linear motion guide. The torque of the electric motor is converted to the vertical force F_d, which acts at point D located at a distance l_d from point O. Here, the structure of the motorized stage is modeled using an equivalent mass m_c, and equivalent moment of inertia J_c with respect to point O, torsional spring k_θ, and torsional damper c_θ.

Figure 3 shows the overall schematic of the lumped model of a conventional AFM system, including the motorized stage. The supporting frame and base plate are considered as rigid bodies, respectively, since they are designed to be very stiff. It is also assumed that the z scanner can be treated as a rigid body since it has a high stiffness; hence, the mass of the z scanner can be combined with the supporting frame. In addition, the spring coefficient of the cantilever is modeled as k_{can} since its mass is negligibly small. Furthermore, the *xy* scanner is considered a rigid body having a mass m_s and a

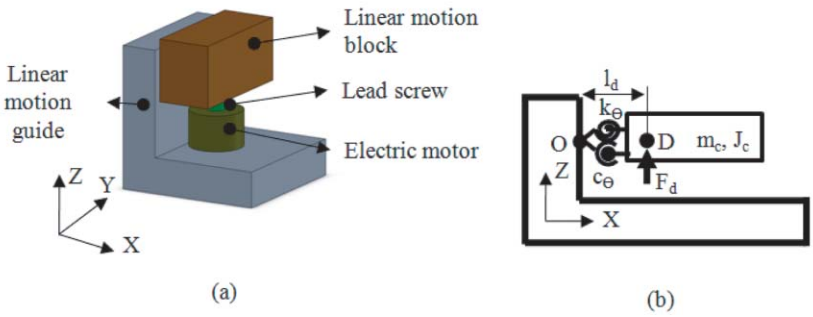

FIG. 2. (Color online) (a) Structure and (b) schematic lumped model of the motorized stage, comprised of a linear motion block, lead screw, electric motor, and linear motion guide.

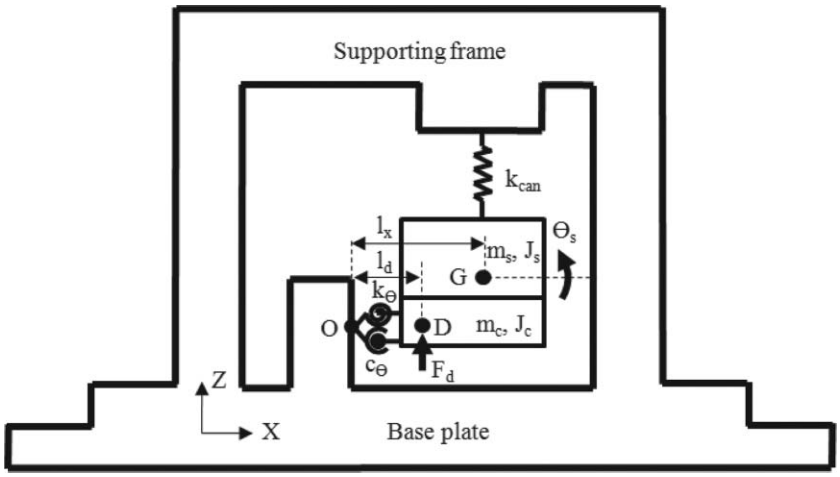

FIG. 3. Overall schematic of the lumped model of a conventional AFM system, including the motorized stage.

moment of inertia J_s with respect to point O; its spring effect in the vertical direction is not considered since it also has a high stiffness compared to that of the lateral direction. And since the xy scanner is mounted on the motorized stage, its mass can be simply added to m_c. Note that the centers of gravity of both m_c and m_s are located at point G, and the distance between points O and G is marked with l_x.

From the model obtained from the above assumptions, the moment equation of the AFM system at point O is represented as

$$(J_s + J_c)\ddot{\theta}_s = -k_\theta \theta_s - c_\theta \dot{\theta}_s + l_d F_d, \tag{1}$$

where θ_s is the output angle with respect to point O. In addition, J_c and m_c are negligibly small compared to J_s and m_s, and J_s is represented as Km_s, where K is the geometrical constant of the xy scanner. Therefore, the transfer function $\theta_s(s)/[l_d F_d(s)]$ can be represented as

$$\frac{\theta_s(s)}{[l_d F_d(s)]} = \frac{1/(Km_s)}{s^2 + 2\zeta\omega_n s + \omega_n^2}. \tag{2}$$

Here, ω_n and ζ are the natural frequency and damping ratio of the AFM system, respectively, which can be represented

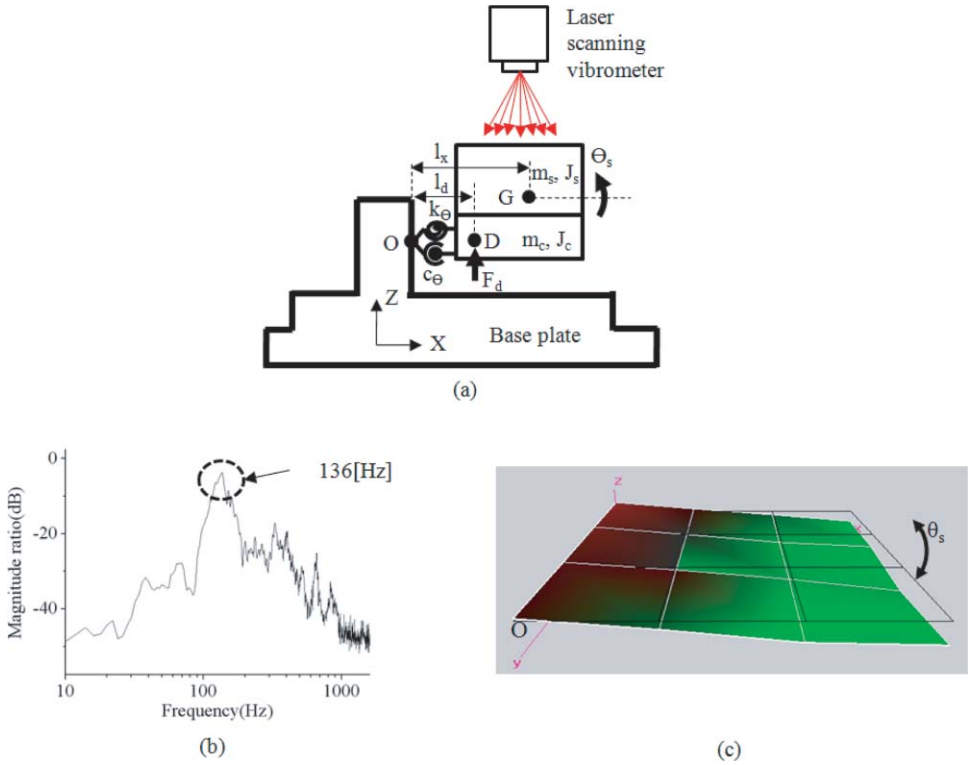

FIG. 4. (Color online) Modal analysis experiment to determine k_θ and c_θ: (a) experimental setup, (b) first bending modal frequency, and (c) first bending mode shape.

Parameter	Description	Value
m_s, J_s	Mass and moment of inertia with respect to point O of the xy scanner	1.3 *kg*, 0.00754 *kg* m^2
K	Geometrical constant of the xy scanner	0.069 m^2
k_θ, c_θ	Torsional spring and damping constants of the motorized stage	5505.6 Nm/rad, 0.947 $Nm/(rad/s)$

FIG. 5. (Color online) Real values of parameters in Eqs. (2) and (3).

as

$$\omega_n = \sqrt{\frac{k_\theta}{K m_s}}, \quad \zeta = \frac{c_\theta}{2\sqrt{K m_s k_\theta}}. \tag{3}$$

As such, in order to reduce the vibration of θ_s, it is necessary to increase the natural frequency and the damping ratio of the AFM system. According to Eqs. (2) and (3), the natural frequency ω_n and damping ratio ζ of the AFM system depend on m_s, k_θ, and c_θ. Therefore, reduction of m_s can contribute to an increase of not only ω_n but also ζ.

In order to experimentally determine k_θ and c_θ, a modal analysis experiment was performed using a laser scanning vibrometer manufactured by EM4SYS Co. Ltd.[21] Figure 4(a) shows the experimental setup of the motorized stage without the supporting frame, since the supporting frame does not interfere with the dynamic characteristics of the motorized stage. The first bending mode occurs at 136 Hz, as shown in Figs. 4(b) and 4(c), and the damping ratio ζ can be estimated as 0.0735 from the half-power bandwidth method.[22] The torsional spring constant $[k_\theta = (\omega_n)^2 J_s]$ and damping constant $(c_\theta = 2\zeta\omega_n J_s)$ are estimated as 5505.6 N m/rad and 0.947 N m/(rad/s), respectively. The real values of the parameters in Eqs. (2) and (3) are listed in Fig. 5.

From the parameter identification of k_θ and c_θ, the simulated result of Eq. (2) is shown in Fig. 6 for a variance of m_s. The damped natural frequency ω_d and damping ratio ζ increase to 299 Hz and 0.16, respectively, when m_s is reduced by a factor of 5. This result confirms that a reduction in the payload of the motorized stage is very important to the vibration attenuation capability of a high speed and high precision AFM.

III. RECONFIGURATION OF MECHANICAL COMPONENTS FOR VIBRATION REDUCTION

In the previous section, it was suggested that m_s should be reduced to attenuate the vibration of θ_s. However, it is not easy to reduce m_s without affecting the design specifications of the xy scanner such as the working stroke and overall size. Without changing the basic design of the xy scanner, we instead propose a reconfiguration of the components in order to obtain a similar vibration attenuation performance.

Figures 7(a) and 7(b) show the structure and schematic of the lumped model of the reconfigured AFM system, respectively. In this model, the motorized stage is located beneath the horizontal supporting frame, and the xy scanner is mounted on the base plate. Then, the motorized stage moves down the z scanner to make contact with the sample surface; different from the previous configuration in which it moves up the xy scanner. In this new configuration, the z scanner, which has mass m_f and moment of inertia J_f with respect to point O, is only a payload for the motorized stage, in which m_f is approximately 1/5 of m_s. Note that the z scanner, xy scanner, and supporting frames have high stiffness, and can therefore be treated as rigid bodies. Then, since the xy scanner is mounted on the base plate, its mass m_s does not need to be considered.

For the vibration analysis of the reconfigured AFM system, its moment equation at point O can be represented as

$$(J_f + J_c)\ddot{\theta}_f = -k_\theta\theta_f - c_\theta\dot{\theta}_f + l_d F_e, \tag{4}$$

where θ_f is the output angle with respect to point O, and F_e is the applied force from the motorized stage to point E, which is located on the supporting frame. The transfer function

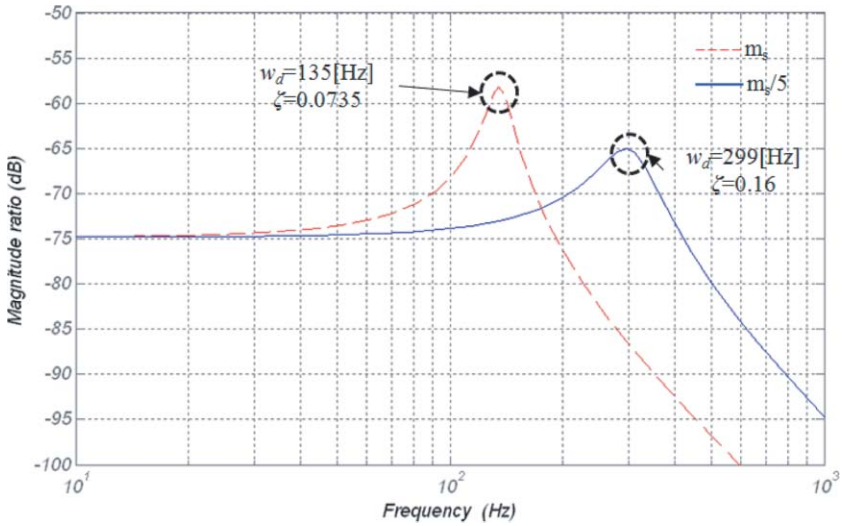

FIG. 6. (Color online) Simulated results of Eq. (2) for a variance of m_s.

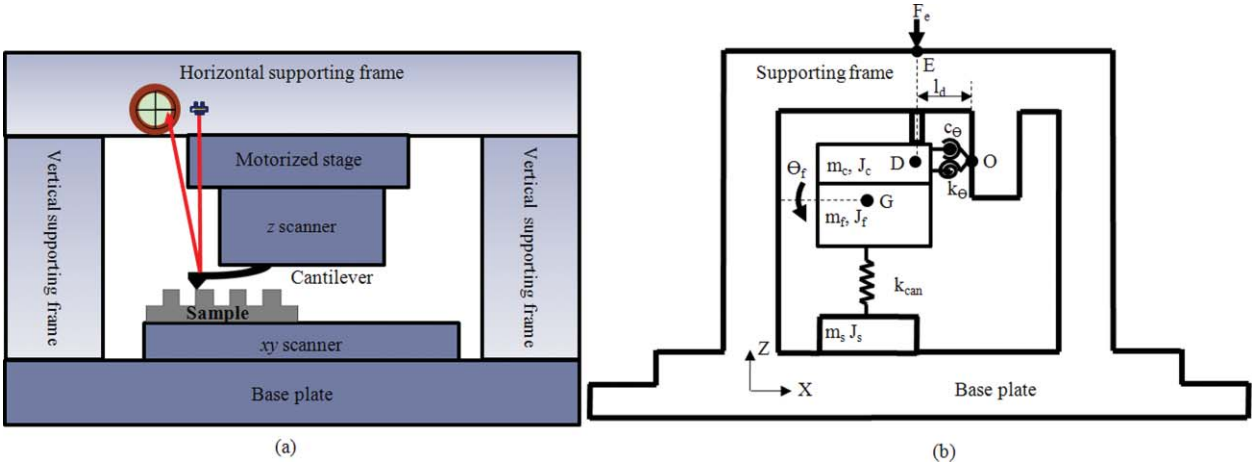

FIG. 7. (Color online) (a) Structure and (b) schematic of the lumped model for the reconfigured AFM system.

$\theta_f(s)/[l_d F_e(s)]$ is then represented as

$$\frac{\theta_f(s)}{[l_d F_e(s)]} = \frac{1/(\tilde{K} m_f)}{s^2 + 2\tilde{\zeta}\tilde{\omega}_n s + \tilde{\omega}_n^2}, \tag{5}$$

where $\tilde{K}$ is a geometrical constant. In addition, $\tilde{\omega}_n$ and $\tilde{\zeta}$ are the natural frequency and damping ratio of the reconfigured AFM system, respectively, which can be represented as

$$\tilde{\omega}_n = \sqrt{\frac{k_\theta}{\tilde{K} m_f}}, \quad \tilde{\zeta} = \frac{c_\theta}{2\sqrt{\tilde{K} m_f k_\theta}}. \tag{6}$$

The frequency response function (FRF) is then experimentally obtained (Fig. 8), in which the *xy* scanner and cantilever are not considered since they do not affect the vibration characteristics of the reconfigured AFM system. The first mode occurs at a higher frequency than that of the previous AFM configuration, where the motorized stage is located below. Indeed, the first mode (291 Hz) almost agrees with that of the simulated frequency response. The second mode (542 Hz) is considered to be attributed to the supporting frame. And the first natural frequency of 291 Hz is the result of reducing the mass by the factor of 5 in the previous AFM configuration, as expected from the simulated results shown in Fig. 6.

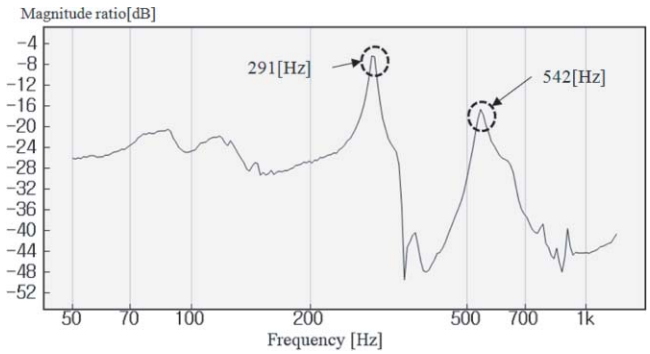

FIG. 8. Experimentally obtained FRF of the reconfigured AFM system.

IV. EXPERIMENTS

Figure 9(a) shows the vertical vibration characteristics due to internal or external disturbances, which in the previous AFM system are measured by the optical sensing signal of the cantilever at a particular point on the sample surface without moving the *xy* scanner. Figure 9(b) shows the measured FFT results of vertical vibration. Here, the natural vibration frequency is observed at 136 Hz, which agrees well with the simulated and experimental results of FRFs. Figure 9(c) then shows the vertical vibration characteristics of the reconfigured AFM system obtained as in the previous AFM system. And Fig. 9(d) shows the measured FFT results of the vertical vibration. The vibration amplitude for the previous AFM system was 4.5 nm peak to peak, whereas it is less than 0.5 nm peak to peak in the reconfigured AFM system. This reduction in amplitude leads to considerable improvement in the image accuracy of the reconfigured AFM system.

Figure 10 presents real scanning images from the AFM for each configuration. The measured standard grid sample has a 3 μm periodic square shape and 12 nm height. Note that even though the *xy* scanner is working in this experiment, it can be concluded that the reconfigured system has a higher performance in image accuracy due to its better vibration attenuation capability.

V. CONCLUSION

The importance of the motorized stage, the most dominant component affecting the accuracy of the AFM, was addressed in this paper. Since the mass mounted on the motorized stage was excessively high in the previous AFM system, the vibration characteristics became degraded. However, instead of designing a new lighter *xy* scanner to be loaded on the motorized stage, vibration reduction was

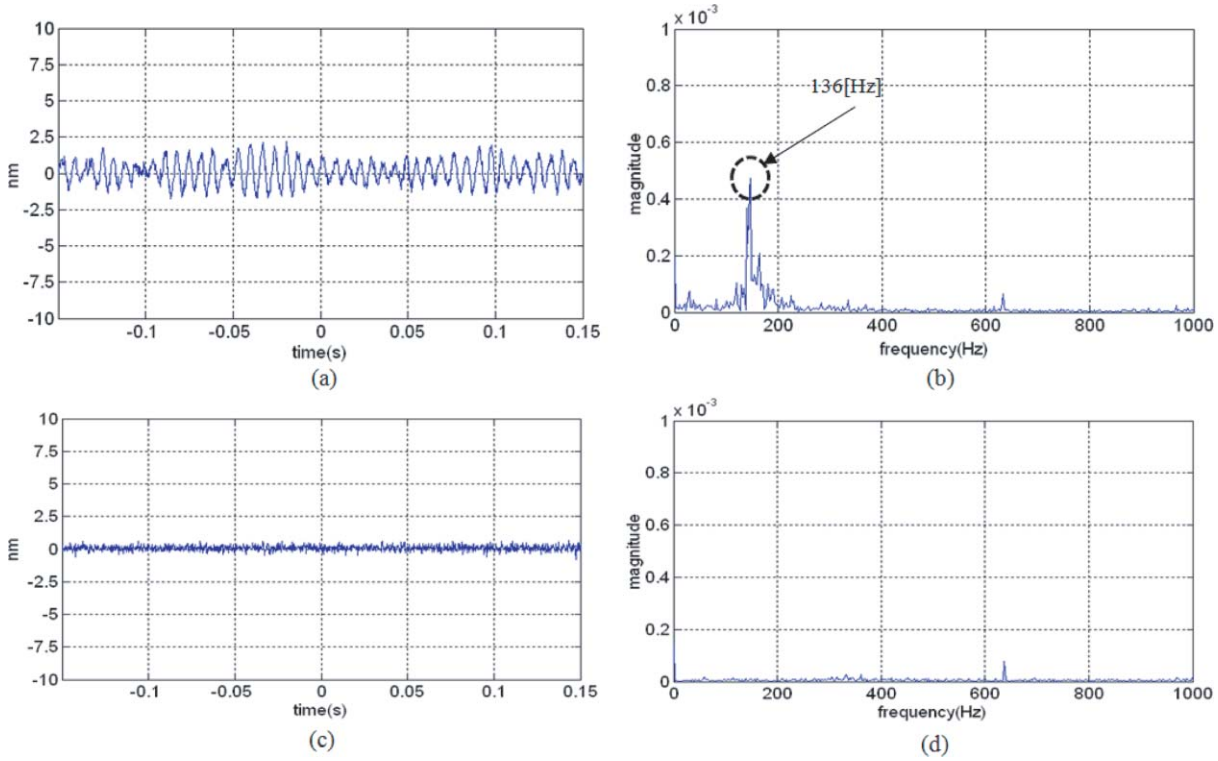

FIG. 9. (Color online) (a) Vertical vibration characteristics due to internal or external disturbances, which in the previous AFM system are measured by the optical sensing signal of the cantilever at a particular point on the sample surface without moving the *xy* scanner. (b) Measured fast Fourier transform (FFT) results of (a). (c) Vertical vibration characteristics of the reconfigured AFM system obtained as in the previous AFM system. (d) Measured FFT results of (c).

achieved by reconfiguring the mechanical components. The reconfigured AFM system helped to reduce the equivalent mass of the motorized stage, which subsequently contributed to increasing the natural frequency and damping ratio of the AFM. Finally, by comparing the vibration of the cantilever of the reconfigured AFM system with that of a previous AFM system at a particular point on the sample surface without moving the *xy* scanner, it was demonstrated that the vibration attenuation capability of the reconfigured AFM system was significantly improved.

ACKNOWLEDGMENTS

This work was supported by the Research Center for Biomolecular Nanotechnology at the Gwangju Institute of Science and Technology, South Korea (Grant No. K02035).

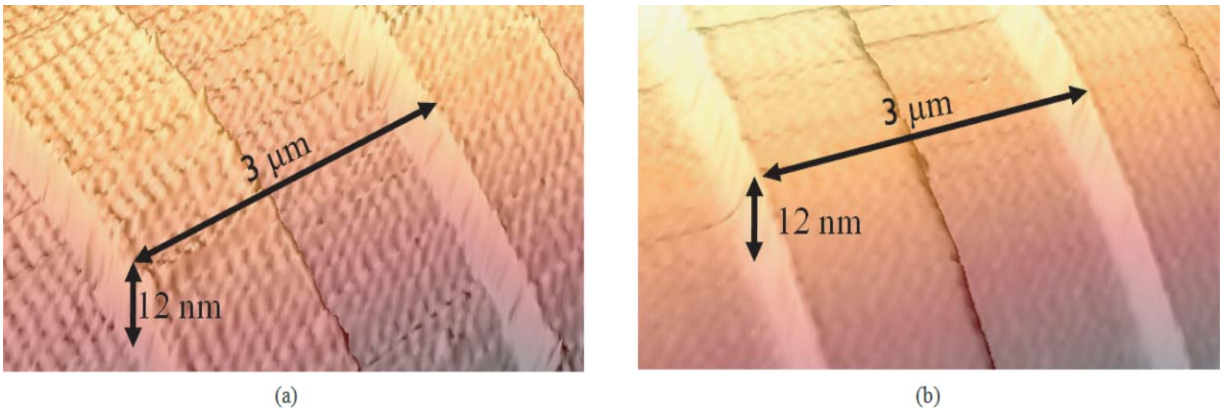

FIG. 10. (Color online) Real scanning images of the (a) previous and (b) reconfigured AFM systems.

[1]G. Binning, C. Berber, E. Stoll, T. R. Alebrecht, and C. F. Quate, Europhys. Lett. **3**, 1281 (1987).
[2]K. Wildeer, C. F. Quate, B. Singh, and D. F. Kyser, J. Vac. Sci. Technol. B **16**, 3864 (1998).
[3]E. Betzig, J. K. Trautman, R. Wolfe, E. M. Gyorgy, P. L. Finn, M. H. Kryder, and C. H. Cahang, Appl. Phys. Lett. **61**, 142 (1992).
[4]J. B. Thomson, B. Drake, J. H. Kindt, J. Hoskins, and P. K. Hansma, Nanotechnology **12**, 394 (2001).
[5]J. Chen, T. Guo, X. Hu, and X. Hu, J. Vac. Sci. Technol. B **27**, 1413 (2009).
[6]J. H. Kindt, G. E. Fantner, J. A. Cutroni, and P. Hansma, Ultramicroscopy **100**, 259 (2004).
[7]G. Schitter, K. J. Astrom, B. E. DeMartini, P. J. Thurner, K. L. Turner, and P. K. Hansma, IEEE Trans. Control Syst. Technol. **15**, 906 (2007).
[8]G. E. Fantner, G. Schitter, J. H. Kindt, T. Ivanov, K. Ivanova, R. Patel, N. Holten-Anederson, J. Adams, P. J. Thurner, I. W. Rangelow, and P. K. Hansma, Ultramicroscopy **106**, 881 (2006).
[9]A. J. Flemming, B. J. Kenton, and K. K. Leang, Ultramicroscopy **110**, 1205 (2010).
[10]G. Schitter, Proceedings of the 2007 American Control Conference, New York, July 11–13, 2007, pp. 3503–3508.
[11]G. K. Binning and D. Smith, Rev. Sci. Instrum. **58**, 1688 (1986).
[12]O. M. E. Riafai and K. Youcef-Toumi, Proceedings of the 2003 American Control Conference, Cambridge, USA, July 4–6, 2003, pp. 3714–3719.
[13]S. Tien, Q. Zou, and S. Devasia, IEEE Trans. Control Syst. Technol. **13**, 921 (2005).
[14]D. Y. Abramovitch, S. B. Anderson, L. Y. Pao, and G. Schitter, Proceedings of the 2007 American Control Conference, New York, July 11–13, 2007, pp. 3488–3502.
[15]J. Kwon, J. Hong, Y. Kim, D. Lee, K. Lee, S. Lee, and S. Park, Rev. Sci. Instrum. **74**, 4378 (2003).
[16]R. Curtis, T. Mitsui, and E. Ganz, Rev. Sci. Instrum. **68**, 2790 (1997).
[17]A. Sebastian and S. M. Salapaka, IEEE Trans. Control Syst. Technol. **13**, 868 (2005).
[18]T. Ando, N. Kodear, E. Takai, D. Maruyama, K. Saito, and A. Toda, Proc. Natl. Acad. Sci. U.S.A. **98**, 12468 (2001).
[19]C. A. J. Putman, B. G. De Grooth, N. F. Van Hulst, and J. Greve, J. Appl. Phys. **72**, 6 (1992).
[20]H. Butt, B. Cappella, and M. Kappl, Surf. Sci. Rep. **59**, 1 (2005).
[21]EM4SYS Co., http://www.em4sys.com., LSV-110D.
[22]A. F. Seybert, J. Sound Vib. **75**, 199 (1981).